Direct Infrared Detection of the Covalently Ring Linked His−Tyr Structure in the Active Site of the Heme−Copper Oxidases†

Farol Tomson,‡ James A. Bailey,§ Robert B. Gennis,‡ Clifford J. Unkefer,|| Zizhong Li,||,⊥ Louis A. Silks,|| Rodolfo A. Martinez,|| Robert J. Donohoe,§ R. Brian Dyer,§ and William H. Woodruff*,▽

Department of Chemistry, University of Illinois at Urbana−Champaign, Urbana, Illinois 61801, and Michelson Resource, Bioscience Division, Los Alamos National Laboratory, C-SIC, MS J568, Chemistry Division, Los Alamos National Laboratory, and National Stable Isotope Resource, Szilard Resource, Bioscience Division, Los Alamos National Laboratory, Los Alamos, New Mexico 87545

Received June 28, 2002; Revised Manuscript Received September 27, 2002

ABSTRACT: Infrared spectroscopy, isotopic labeling ([$^{15}N_{\delta,\epsilon}$]histidine and ring-deuterated tyrosine), synthetic model studies, and normal mode calculations are employed to search for the spectroscopic signatures of the unique, covalently linked (His $N_\epsilon-C_\epsilon$ Tyr) biring structure in the heme−copper oxidases. The specific enzyme examined is the cytochrome *bo*$_3$ quinol oxidase of *E. coli*. Infrared features of histidine and tyrosine are identified in the frequency regions of imidazole and phenol ring stretching modes (1350−1650 cm^{-1}) and C−H and N−H stretching modes as well as overtones and combinations (>3000 cm^{-1}). Two of these, at ca. 1480 and 1550 cm^{-1}, and their combination tones between 3010 and 3040 cm^{-1}, are definitively identified with the biring structure involving H284 and Y288 in the *E. coli* enzyme. Studies of a synthetic analogue of the H−Y structure, 4-methylimidazole covalently linked to *p*-cresol, show that a feature near 1540 cm^{-1} is unique to the biring structure and is absent from the infrared spectrum of 4-methylimidazole or *p*-cresol alone. This feature is readily detectable by infrared difference techniques, and offers a direct spectroscopic probe for potential radical production involving the H−Y structure in the O_2 reduction cycle of the oxidases.

The heme−copper oxidases, which occur in aerobic organisms from archae and bacteria to humans, comprise an enzyme superfamily that is responsible for more than 90% of the biological dioxygen reduction on earth. The reaction that they catalyze, between a proximate electron donor and O_2 to produce H_2O, accounts for approximately half of the total energy of aerobic respiration. The mechanisms by which these oxidases activate O_2 and conserve the energy of the O_2 reduction for subsequent ATP synthesis constitute one of the major issues in bioenergetics.

The universally conserved functional apparatus of the heme−copper oxidases resides in "subunit I" of these multiple-subunit enzymes, and consists of one isolated heme with two axial histidine imidazole ligands and a heme−copper binuclear site composed of a heme with one axial histidine imidazole ligand (heme a_3, o_3, or b_3) and a nearby copper ion normally liganded by three histidine imidazoles (Cu_B). Crystallographic results over the past few years (*1*−*7*) have focused attention on specific structures, side chains, channels, and redox cofactors that may be significant in the redox sequence and, in particular, in the mechanisms of energy conservation by transmembrane proton translocation.

The location where substrate O_2 binds and is reduced is the binuclear site composed of the five-coordinate heme and Cu_B, but the nature of the redox intermediates involved, and especially the ligation and protonation steps and the way in which the redox energy is coupled to that required for proton translocation, is not well established. Subsequently to the original structure determinations, crystallographic refinements (*4*, *5*) have revealed that a unique macrocyclic peptide structure exists at the active site and contains some of the key, functionally significant amino acids of the enzyme. This structure consists of one turn of the α-helix composed of the highly conserved residues (residue numbers given are for *E. coli* cytochrome *bo*$_3$) H284, P285, E286, V287, and Y288. The macrocyclic unit is completed by a covalent bond between N_ϵ of H284 and C_ϵ (*ortho* to the phenolic OH) of Y288. In addition, H284 serves as one of the three endogenous ligands of Cu_B via a bond between N_δ and the copper ion. The existence of this histidine−tyrosine linked structure in the active form of the enzyme has been confirmed by protein chemical analysis (*8*) and is therefore not a result of, for example, X-ray-induced coupling occurring during crystal structure determination.

The covalent link between H284 and Y288 is obviously a post-translational modification, and it is virtually certain that this bond forms as a result of radical coupling chemistry

† We are grateful for support by grants from the National Institutes of Health (DK36263 to W.H.W. and RR22031 to C.J.U.) and the U.S. Department of Energy (DEFG02-87ER13716 9 to R.B.G.).

* To whom correspondence should be addressed. Phone: (505) 667-2557. Fax: (505) 667-0851. E-mail: woody@lanl.gov.

‡ University of Illinois at Urbana−Champaign.

§ Michelson Resource, Bioscience Division, Los Alamos National Laboratory.

|| Szilard Resource, Bioscience Division, Los Alamos National Laboratory.

⊥ Present address: Medical Department, Brookhaven National Laboratory, P.O. Box 5000, Upton, NY 11973.

▽ Chemistry Division, Los Alamos National Laboratory.

10.1021/bi026370c CCC: $22.00
Published on Web 11/09/2002

initiated by strongly oxidizing oxygen species formed during the early O_2 turnover reactions of the assembling enzyme (*9*). Given that side chain radicals of H284/Y288 are energetically accessible during O_2 turnover, as the coupling reaction suggests, the prospect that radical formation is a general mechanistic feature of O_2 turnover has been suggested (*10*−*12*). The possibility that this might occur could provide a key to understanding the aspects of proton translocation as well as the redox sequence during turnover, and experimental probes that might detect side chain radicals in situ during the O_2 reactions are vitally important to test this possibility. While indirect chemical evidence exists based on iodine trapping by putative radical species and subsequent amino acid analysis (*13*), no direct experimental probe for observing radical production and behavior during turnover has yet emerged.

In recent years several studies have appeared that employ infrared spectroscopy to probe the responses of the peptide backbone, side chains, and redox cofactors of heme−copper oxidases to various perturbations including ligation, protonation, and electron transfer (*14*−*17*). These studies have clearly established that IR has the sensitivity and resolution, when employed in a difference mode, to detect spectral changes in individual chemical bonds or side chain substructures within oxidase enzymes that have a relative molecular mass of 250000 or greater. In addition, the IR differences, which reflect changes in bond strengths and effective masses or atomic positions, are easily interpreted in terms of structural changes within the protein. The problem is how to identify the spectral changes with the specific structures, e.g., amino acid residues, when the protein has 10^4 to 10^5 normal vibrational modes, all of which may be IR active. In some cases this can be done by site-directed mutation (*14*), but in others isotopic substitution is necessary (*18*). The difference spectra in each of these cases are essentially identical except for the specific features that shift in response to the mutation or the change in isotopic mass. Thus, a "double-difference" spectrum reveals shifts in band positions that belong to the residue(s) that have been altered *and* are sensitive to the externally applied perturbation.

In the present work we use isotopic substitution on histidine and tyrosine, combined with infrared studies of the difference spectra generated by low-temperature photodissociation of CO from the o_3 heme of cytochrome bo_3 (the quinol oxidase from *E. coli*), to identify features in the IR spectra that are sensitive to the CO photodissociation and in addition exhibit isotope shifts. Features are seen in the IR frequency range 1350−1650 cm^{-1} that satisfy both criteria, and these are definitively assigned to histidine imidazole (in the case of $^{15}N_{\delta,\epsilon}$ substitution) or to the phenol ring of tyrosine (in the case of ring deuteration at the *ortho* and *meta* positions). These observations, however, merely allow us to identify some peaks due to histidine and tyrosine, not to identify the specific features due to the linked H284−Y288 (H−Y) structure. In parallel, we have employed computational methods to calculate vibrational normal modes of natural isotopic abundance (NA)[1] and isotopically labeled models to assist in identification of vibrations and isotopic shifts pertinent to the linked biring structure. These results have also provided insight into the substructures that are involved in each mode and, in particular, any mode that involves the C−N bond that constitutes the H−Y link. In addition, we synthesized the covalent biring complex of 4-methylimadazole and *p*-cresol, linked via a bond between the N(1) of the imidazole and the carbon of *p*-cresol *ortho* to the phenolic OH. Infrared study of this synthetic model reveals unique features of the spectrum that are not present in either 4-methylimidazole or *p*-cresol alone. This guides the protein observations and provides indicative evidence for assigning at least one of the isotope-sensitive modes to the H−Y structure.

MATERIALS AND METHODS

Materials. Unless otherwise noted, commercial chemicals were used without further purification. L-[*ring*-$^2H_4$]Tyrosine, [*ring*-$^{15}N_2$]histidine, and methyl[$^{15}N_2$]imidazole were provided by the National Stable Isotope Resource at Los Alamos National Laboratory.

Synthesis of the His−Tyr Model. In addition to the synthesis reported here, others have reported syntheses of covalently linked imidazole−phenol structures (*24*, *25*). While the objective in all cases was to produce synthetic mimics of the covalently linked H−Y structure in the oxidases, the details of the synthetic approaches are significantly different.

Reactions were performed under an argon atmosphere using glassware previously dried in an oven at 120 °C. Tetrahydrofuran (THF) and dichloromethane were freshly distilled from benzophenone ketyl and calcium hydride, respectively. Benzene was dried over 3 Å sieves. Flash column chromatography was performed using silica gel 60 (230−400 mesh). Silica gel thin-layer chromatography was done on plates (silica gel 60, F254, 0.15 mm). NMR spectra were obtained at 7.05 T (300 MHz, ^1H) or 11.7 T (500 MHz, ^1H). Unless otherwise noted, samples were dissolved in chloroform-*d* with TMS as an internal standard.

*2-Bromo-1-(methoxymethoxy)-4-methylbenzene (***2***)*. 2-Bromophenol (**1**) (9.30 g, 53.8 mmol) was added dropwise at 0 °C to a stirred suspension of sodium hydride (5.00 g of a 50% dispersion in mineral oil) in anhydrous THF (150 mL). After hydrogen evolution ceased (∼1.5 h), the solution was stirred for an additional 0.5 h, and then chloromethyl methyl ether (5.00 g, 62.1 mmol) was added dropwise. The reaction mixture was then stirred overnight at room temperature. The reaction mixture was diluted with ether (150 mL), washed with water (3 × 30 mL), and then dried over $MgSO_4$. The mixture was filtered through silica gel and evaporated in vacuo to give 11.5 g of **2** (93%): ^1H NMR δ 7.41 (m, 1H), 7.08 (m, 2H), 5.26 (s, 2H, CH_2), 3.56 (s, 3H, CH_3), 2.31(s, 3H, CH_3); ^{13}C NMR δ 151.6, 133.8, 133.0, 128.9, 116.4, 112.7, 95.3, 56.3, 20.2.

*2-Methoxymethoxy-5-methylphenylboronic Acid (***3***)*. **2** (1.80 g, 7.79 mmol) was dissolved in a mixture of 50 mL of dry benzene and 50 mL of dry THF, and the solution was cooled to −78 °C. A 3.7 mL (8.51 mmol) aliquot of a 2.3 M solution of *n*-butyllithium in hexane was added. In a separate flask, 3.91 mL (40.6 mmol) of trimethyl borate was added to 20 mL of THF, and the mixture was cooled to −78 °C. This solution was then transferred to the carbanion

[1] Abbreviations: d_4-Y, ring-deuterated tyrosine; FTIR, Fourier transform infrared; MCT, mercury cadmium telluride; MOM, methoxymethyl; NA, natural isotopic abundance.

solution. The resulting mixture was slowly warmed to room temperature. Water (20 mL) was added slowly to destroy excess *n*-butyllithium. The THF was evaporated under reduced pressure, and the residue was extracted with ether (3 × 30 mL). The combined organic layer was washed with 3 M NaOH (3 × 20 mL). The aqueous layer was acidified with 3 M HCl and then extracted with ether (3 × 30 mL). The organic layer was washed with brine, dried over magnesium sulfate, and evaporated to give 1.30 g (85%) of **3** as a waxy solid: ^{1}H NMR (DMSO-d_6) δ 7.35(d, 1H, J = 2.7 Hz), 7.14 (dd, 1H, ^3J = 9.3 Hz, ^4J = 2.7 Hz), 4.95 (s, 2H), 6.95 (d, 1H, J = 9.3 Hz), 3.37 (s, 3H), 2.22 (s, 3H); ^{13}C NMR (DMSO-d_6) δ 159.4, 136.1, 132.0, 130.3, 114.4, 94.8, 56.1, 20.6.

*2-(4-Methyl-1H-imidazol-1-yl)-1-(methoxymethoxy)-4-methylbenzene (***4***)*. A 50 mL round-bottom flask was charged with **3** (200 mg, 1.00 mmol), 4-methylimidazole (120 mg, 1.50 mmol), anhydrous cupric acetate (408 mg, 2.25 mmol), 0.60 g of 4 Å molecular sieves, pyridine (2.0 mL of a 1 M solution in dichloromethane), and 20 mL of dichloromethane. The mixture was stirred at ambient temperature for 3 days. The reaction mixture was filtered through Celite, diluted with ether (100 mL), washed with water, and then dried over sodium sulfate. The solvent was evaporated, and the residue was purified by silica gel chromatography (95/5 dichloromethane/methanol, v/v) to give 90 mg of **4** (39%): ^{1}H NMR δ 7.76 (br s, 1H), 7.20 (d, 1H, J = 9.3 Hz), 7.14 (m, 2H), 6.9 (br s, 1H), 5.15 (s, 2H), 3.44 (s, 3H), 2.38 (s, 3H), 2.34 (br s, 3H); ^{13}C NMR δ 148.0, 137.0, 132.3, 129.0, 127.5, 126.1, 116.7, 95.3, 56.2, 20.4, 13.6.

*2-(4-Methyl-1H-imidazol-1-yl)-4-methylphenol (***5***)*. Pyridinium *p*-toluenesulfonate (1.50 g) was added to a solution of **4** (700 mg, 3.01 mmol) in *tert*-butyl alcohol (20 mL). The mixture was refluxed for one week while being monitored for completion by TLC. The solvent was evaporated, and the residue was purified by silica gel chromatography (95/5 dichloromethane/methanol, v/v) to give 480 mg (84%) of **5** and 100 mg (14%) of **4**: ^{1}H NMR δ 7.44 (s, 1H), 7.05 (dd, 1H, J = 8.30 Hz, J = 1.85 Hz), 6.99 (d, 1H, J = 8.30 Hz), 6.91 (d, 1H, J = 1.85 Hz), 6.78 (s, 1H), 2.26 (s, 3H), 2.12 (s, 3H); ^{13}C δ 149.4, 137.3, 136.7, 130.2, 129.4, 126.5, 124.7, 118.5, 116.6, 20.3, 13.0; HMRS calcd for $C_{11}H_{12}N_2O$ 188.0950, found 188.0948.

Culture Conditions. The auxotrophic *E. coli* strains were grown in M63 minimal medium with added copper, antibiotic, carbon source, and the necessary substrate. M63 minimal medium contains 100 mM KH_2PO_4, pH 7.0, 15 mM $(NH_4)_2SO_4$, 5 M $FeSO_4{\cdot}7H_2O$, 100 mg/L thiamine, and 10 mM $MgSO_4$. The *E. coli* oxidase requires copper and is grown in lactate: 0.03 mM $CuSO_4$ and 0.3% lactate.

The histidine auxotroph strain, HfrG11 (*19*), was transformed with pJRHisA. The plasmid pJRHisA contains the *bo*$_3$ oxidase genes *CyoA*−*CyoE* with a six-histidine tag attached to the end of *CyoA* (*20*). The histidine tag is used in affinity purification using a Ni^{2+} column. This strain was grown in M63 medium with 0.3% lactate, 0.3% glycerol, 100 mM $CuSO_4$, 100 mg/L ampicillin, and either 100 mg/L [*ring*-$^{15}N_2$]histidine or 100 mg/L unlabeled histidine. The tyrosine auxotroph, WU38 (CGSC no. 5975), was obtained from the *E. coli* Genetic Stock Center, Department of Biology, Yale University. The growth of WU38 transformed with pJRHisA used M63 medium with 0.3% lactate, 0.3% glycerol, 100 mM $CuSO_4$, 100 mg/L ampicillin, and either 100 mg/L L-[*ring*-$^2H_4$]tyrosine or 100 mg/L unlabeled tyrosine.

Sample Preparation. Purified protein was obtained by following established protocols (*20*). The protein samples were transferred to the following buffer used for FTIR experiments by using a centrifugation concentrator: 400 μM enzyme, 100 mM HEPES or potassium phosphate, pH 7.4, 0.1% *n*-dodecyl-D-maltoside, and 5% glycerol in D_2O. The samples were diluted and concentrated three times to ensure the buffer was completely exchanged. The IR sample cell consisted of two round 25 mm CaF_2 windows with a 15 μm spacer. The enzyme was equilibrated under a stream of argon, and a small amount of concentrated dithionate solution was added to reduce the enzyme. The gas above the enzyme was changed to CO and allowed to equilibrate for at least 15 min to ensure complete binding of the CO to the heme. The sample was loaded into the presealed Ar-purged cell using a gastight syringe. After loading, the sample was checked in a UV−vis spectrometer to make sure the enzyme was reduced and had bound CO.

Low-Temperature CO Photolysis FTIR Difference Spectroscopy. Cryogenic FTIR spectra were collected as outlined previously (*15*). Briefly, the sample cell was attached to the cryostat and brought under vacuum. The temperature was maintained at 80 K for the experiments. Up to 12 sets of 64 scans of the protein were taken. These preilluminated scans are considered the "dark" spectra. The sample was irradiated with a frequency-doubled Nd:YAG (532 nm) or Ar^+ (all lines visible) laser for a total of 5−10 mJ. These postillumination spectra are referred to as the "light" spectra. Any further illumination by the laser did not cause the signal of the Cu_B−CO band to increase, indicating complete photolysis. Five to twelve sets of 64 scans of the light spectra were taken. The light and dark spectra were averaged and then used in the light minus dark spectral determination. This entire process was repeated 8−10 times to establish the peak precision and signal-to-noise ratio (S/N). The reproducibility of the peak positions was better than 0.1 cm^{-1}, and photometric noise was less than 1×10^{-5} AU (S/N > 10 for the reported peaks).

To take more spectra, the sample was warmed to 260 K so the CO could rebind to the Fe_{o_3} atom. The sample was then cooled back to 80 K and the process repeated. Normally one sample could survive 2−5 cycles of heating and cooling before the level of photolysis became too small to measure.

Normal Mode Calculations. Vibrational normal modes and IR spectra were calculated using the Hyperchem molecular modeling software. Model structures were built using each of two methods: atom coordinates were either built from amino acid residues and single atoms using the molecular building routines in Hyperchem or loaded from the Brookhaven Protein Database (for bovine cytochrome *c* oxidase). Model structures included *p*-cresol, 4-methylimidazole, compound **5**, and the five-residue helix turn of cytochrome *bo*$_3$ with an H−Y link: His284-Pro285-Glu286-Val287-Tyr288. For the helix model derived from the PDB structure, the data set was truncated to include only the corresponding residues (240−244) in cytochrome *c* oxidase. A proton was added to E286 to match the experimentally determined

Table 1: Observed and Calculated IR Frequencies and Isotopic Shifts for [^{15}N]His- and [^{2}H]Tyr-Substituted Cytochrome bo_3[a]

ν_{obsd} (ν_{calcd}), cm^{-1}	$\Delta\nu_{obsd}$(^{15}N) ($\Delta\nu_{calcd}$(^{15}N)), Δcm^{-1}	$\Delta\nu_{obsd}$(^{2}H) ($\Delta\nu_{calcd}$(^{2}H)), Δcm^{-1}	assignment[b]
1412 (1412)	−15 (−23)	0 (−1)	ring mode substantially localized on His
1483 (1497)	−10 (−13)	0 (−2)	ring mode substantially localized on His (Figure 4a)
1549 (1562)	−9 (−8)	−9 (−13)	coupled His and Tyr ring modes with large inter-ring CN contribution (Figure 4b)
1579 (1603)	−5 (−3)	−9 (−16)	coupled His and Tyr ring modes with large inter-ring CN contribution[c]
3033 (3059)[d]	−23 (−25)[d]	−8 (−15)[d]	combination tone between 1483 and 1549 cm^{-1} bands

[a] Calculated values in parentheses. [b] Assignments from inspection of the calculated displacement vectors. [c] Assignments on the basis of our vibrational calculations, which predict a mode with a large contribution from the ring−ring bond coordinate, and consistent frequency and isotope shifts. [d] Calculated combination bands obtained from simple addition of calculated frequencies for the appropriate fundamentals.

Scheme 1

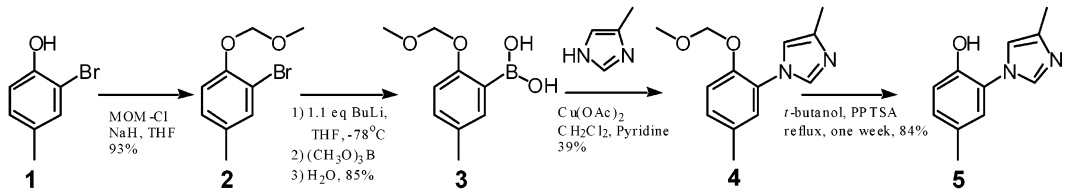

protonation state (*14*). The "hand-built" structure was adjusted manually to ensure a reasonable match to the X-ray conformation, and the H−Y link was added. A number of model structures were built with differing C and N termini. The C terminus was (CO)H, (CO)OH, or an added Gly residue ((CO)OH), and the N terminus was either NH_2 or a Gly residue (NH_2). The geometry of the molecule was then adjusted to an energy minimum using a procedure based on the PM3 semiempirical method (*21*, *22*). The final RMS error between the energy-optimized helix model from X-ray coordinates and the original X-ray structure was 2.78 Å (81 atoms), and for the hand-built helix model and original X-ray coordinates the RMS error was 3.54 Å for 81 atoms. Vibrational normal modes were then calculated using the PM3 method. For isotope substitution calculations, the mass of $^{15}N_{\delta,\epsilon}$ atoms on H240 was set to 15.0011 amu and that of ^{2}H atoms on Y244 to 2.014 amu. A last set of spectra for the isotope-substituted series was calculated with a $Cu^{I}(NH_3)_2$ fragment bonded to N_δ of H240 to simulate Cu_B. The values from these calculations are reported in Table 1. In general, calculations gave similar results (for the corresponding isotope) with differences in calculated frequencies of less than 3 cm^{-1}, except for the modes that show appreciable contribution from the N_δ that would be normally bonded to Cu_B. These modes shift down in energy ($\sim$40 cm^{-1} for the 1497 mode) when the Cu fragment is added.

Vibrational frequencies calculated by either semiempirical or ab initio methods are in most cases larger than the experimentally observed frequencies. Errors in the calculations can be traced to omission of anharmonicity and incomplete electron correlation or configuration interaction. For many methods, a simple scaling factor of the computed results can be employed (*23*). For PM3, the scaling factor of 0.976 was used as determined in ref *23*. Although the absolute energies are often still in error even after application of the scaling factor, assignment of normal modes to the observed spectral bands can often be accomplished. While ab initio methods are usually more accurate than semiempirical methods, there is a high cost in computation time. For the calculated values reported here, the semiempirical method PM3 was employed for all models.

RESULTS

Synthesis of the H−Y Model. Since we initiated these studies, several routes to models of the His−Tyr dimer have been reported (*24*−*26*). Each of the routes is based on a copper-mediated coupling of the imidazole and phenol ring systems. We used a similar approach to prepare the minimal realistic H−Y model for infrared spectroscopy, which must include the imidazole and phenol rings linked at the appropriate atoms with alkyl substituents at the appropriate positions. "H−Y models" lacking the alkyl substituents may be adequate models for other experimental probes such as electrochemistry (*24*) or EPR (*24*, *26*), but vibrational spectroscopy imposes stricter structural requirements on valid models (see the Discussion). The molecule **5** shown in Figure 1 (inset) contains 4-methylimidazole and *p*-cresol substructures covalently linked between N(1) of the imidazole ring and the *ortho* carbon (C2) of the phenol ring. This link mimics the His N_ϵ−C_ϵ Tyr bond in the oxidases, and the methyl groups mimic the β-methylene carbons of His and Tyr.

The H−Y model 2-(4-methyl-1*H*-imidazol-1-yl)-4-methylphenol (**5**) was prepared as outlined in Scheme 1. Briefly, 2-bromophenol (**1**) was converted to the corresponding methoxymethyl (MOM) ether (**2**). The bromide was transmetalated and the resulting carbanion trapped with trimethyl borate. Hydrolysis yielded the boronic acid derivative **3**. A copper-promoted coupling of **3** with 4-methylimidazole followed by removal of the MOM protecting group gave the H−Y model **5**. Using the same scheme and starting with methyl[$^{15}N_2$]imidazole, we prepared the $^{15}N_2$-labeled H−Y model. While coupling of the 4-substituted imidazoles to the aryl ring could potentially give rise to two regioisomers, proton and ^{13}C NMR spectra were consistent with a single product. ^{1}H NMR NOE studies and X-ray crystal data firmly establishing the formation of the N1−C2 bond will be presented elsewhere.

Infrared Spectroscopy. Figure 1 shows the infrared spectrum of **5** in the frequency region 1350−1650 cm^{-1}, along with the spectra of unlinked 4-methylimidazole and *p*-cresol in the same region. Most of the features in the IR spectrum of **5** have counterparts in the spectra of 4-methylimidazole

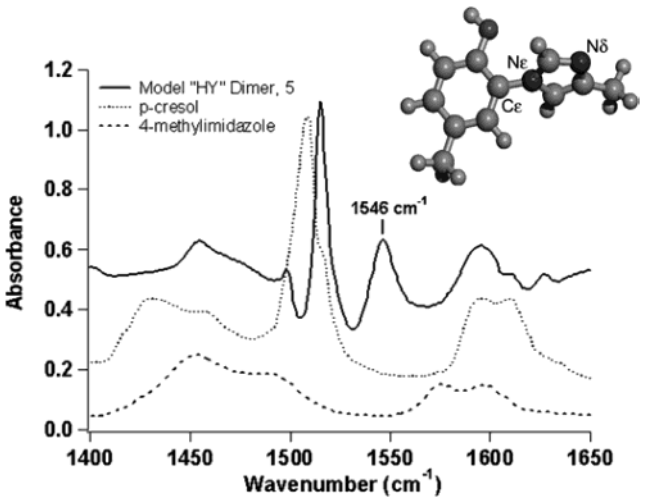

FIGURE 1: FTIR spectra of compound **5** (—, D_2O), *p*-cresol (•••, melt), and 4-methylimidazole (---, melt). Baselines are offset for clarity. (Inset) Model of compound **5** showing the covalent link between 4-methylimidazole and *p*-cresol substructures. Atom labels are as used in the protein structure.

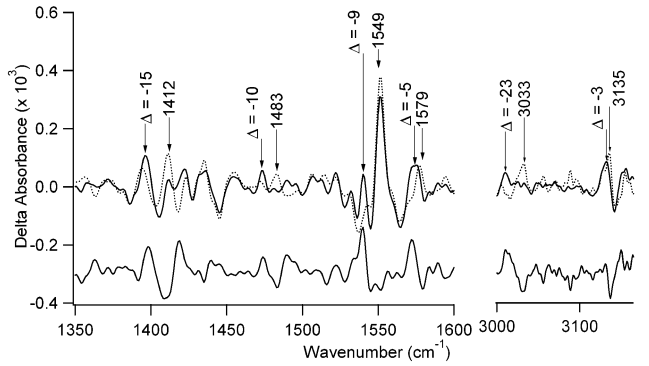

FIGURE 2: FTIR difference spectra of low-temperature CO photolysis (Cu_B−CO minus Fe_{o_3}−CO) of cytochrome *bo*$_3$. Upper traces: natural isotopic abundance (•••) and ^{15}N-labeled histidine (—). Lower trace: double-difference spectrum (^{15}N − NA). (a, left) Low-frequency region. (b, right) High-frequency region.

and *p*-cresol, including the broad peaks near 1450 and 1600 cm^{-1} and the phenolic ring mode near 1510 cm^{-1}. One prominent peak at 1546 cm^{-1} in the spectrum of **5**, however, has no counterpart in the spectra of the unlinked substructures.

Figure 2 shows the photochemical difference spectra (postillumination minus preillumination) of the CO complex of fully reduced cytochrome *bo*$_3$ in D_2O. These experiments are done at 80 K; therefore, the CO is bound to the o_3 heme Fe before illumination and to Cu_B after illumination. Two cytochrome *bo*$_3$ spectra are shown: the wild-type (NA) enzyme and an isotopically labeled derivative wherein both histidine imidazole ring nitrogens (N_δ and N_ϵ) have been substituted by ^{15}N. The isotopic substitution applies to all histidines in the protein. In this figure we show only the high- and low-frequency regions where significant isotopic shifts appear. The frequencies and intensities of most of the IR features in the cytochrome *bo*$_3$ spectra are the same within our experimental error. However, several shifts are evident between the natural abundance and ^{15}N spectra. The most obvious shifts are in four peaks in the low-frequency region (NA frequencies given first), from 1579 to 1574 cm^{-1}, from 1549 to 1540 cm^{-1}, from 1483 to 1473 cm^{-1}, and

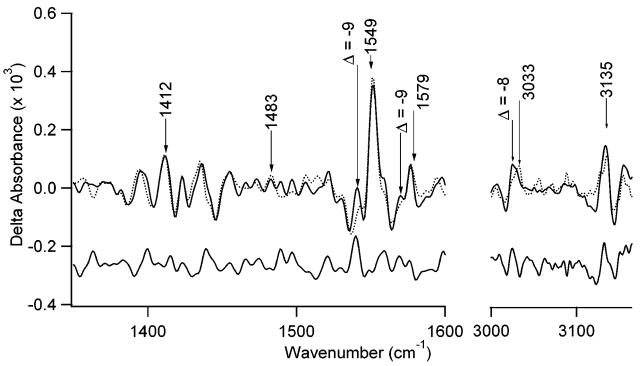

FIGURE 3: FTIR difference spectra of low-temperature CO photolysis (Cu_B−CO minus Fe_{o_3}−CO) of cytochrome *bo*$_3$. Upper traces: natural isotopic abundance (•••) and ^{2}H-labeled tyrosine (—). Lower trace: double-difference spectrum (^{2}H − NA). (a, left) Low-frequency region. (b, right) High-frequency region.

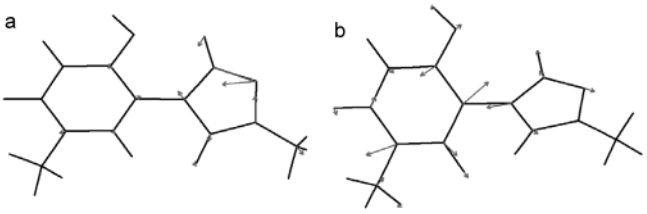

FIGURE 4: Calculated displacement vectors for modes at (a) 1483 cm^{-1} and (b) 1549 cm^{-1}.

from 1412 to 1397 cm^{-1}, and two in the high-frequency region, from 3135 to 3132 cm^{-1} and from 3033 to 3010 cm^{-1}. The 1900−2100 cm^{-1} region where the carbon monoxide stretches appear shows no isotopic shifts (^{15}N or ^{2}H) for either Fe_{o_3}−CO or Cu_B−CO (not shown).

Figure 3 shows the data, as in Figure 2, for incorporation of ring-deuterated tyrosine (d_4-Y) into the cytochrome *bo*$_3$. As expected, because the mass changes are not on atoms integral with the ring, the isotope effects on the spectra are generally neither as large nor as intense as the ^{15}N effects.

Calculated and observed frequencies for bands showing either ^{15}N or ^{2}H shifts are presented in Table 1. In the calculated spectra of all models containing the H−Y link, four bands appeared in the 1400−1650 cm^{-1} region with significant isotope shifts for [$^{15}N_2$]His. For each of these modes, the observed frequency and ^{15}N isotope shift are very similar to the calculated values. For ^{2}H-labeled models, two of these same modes show significant shifts similar in magnitude to those observed. The calculated displacement vectors for two of these modes (1483 and 1549 cm^{-1}) are shown in Figure 4. Details of the assignments are given in the Discussion.

DISCUSSION

The features of the infrared spectra of H284 and Y288 that are expected to be sensitive to radical formation are those involving bonds within the π systems of the rings, namely, the bonds within the rings themselves plus the inter-ring bond (His N_ϵ−C_ϵ Tyr). Some insight into where to look for these vibrations in the proteins can be gained by studying the infrared spectra of synthetic model dimers that embody the essential structural features of the linked H−Y unit. To be a valid H−Y model for the purposes of vibrational spectroscopy, the synthetic compound needs to incorporate (a)

imidazole and phenol rings linked by a covalent bond between the equivalent atoms to the His N_ϵ and the Tyr C_ϵ in H−Y and (b) aliphatic groups in the correct positions (at least the β-carbons) to mimic the His and Tyr side chains in H−Y. The β-carbon substitution is a requirement because the imidazole and phenol ring modes, which are expected to be sensitive to radical formation, may mix with nonring modes (such as the ring−C stretch and the C−H deformations of the β-carbon) such that the vibrational features of the unsubstituted ring systems may not resemble H−Y, resulting in confusion in the assignments.

Although this latter point is not explicitly discussed in ref *26*, it is clearly supported by the IR spectra of the two H−Y model compounds reported therein. The first model (**I**) is histidine linked to an unsubstituted phenol ring by a covalent bond between N_ϵ of His and the *ortho* carbon of the phenol. IR results on this compound are subject to the caveat stated above because the aliphatic substituent mimicking the β-methylene group of Tyr is missing. The second model (**II**) is the similarly linked dimer of His and Tyr. In terms of the vibrational spectroscopy of the H−Y ring−ring system, **II** is obviously a valid model. However, it incorporates the full structural and spectral complexity of its constituent amino acids (instead of simply the ring−ring system), which could obscure important details. The authors note that the spectrum of **I** is significantly different from that of **II** (Figures 7 and 8). Moreover, because the interpretations in ref *26* rely in part on the IR spectra of **I**, and because no isotope shifts were available, important IR signatures of the H−Y structure in the protein (vide infra) were not identified in the spectra of the linked His−Tyr model structure by these authors.

Figure 1 shows the infrared spectrum of **5** and spectra of unlinked 4-methylimidazole and *p*-cresol in the frequency region 1350−1650 cm^{-1}. While most of the bands in the spectrum of **5** can be identified with a corresponding band in the spectra of the unlinked structures, there is one band at 1546 cm^{-1} that appears to be a new feature. This is a likely candidate to be assigned as a unique normal mode of the dimer having substantial contribution from the inter-ring C−N bond stretching coordinate. Thus, in the isotopically labeled enzyme studies, we should consider peaks with frequencies near 1550 cm^{-1} as candidates for the equivalent H−Y modes.

In the past, we and others (*14*−*16*, *27*) have used the photodissociation of CO from the five-coordinate heme in oxidases as a perturbation that shifts the IR frequencies and intensities of many backbone and side chain structures near the heme. Under cryogenic conditions the photodissociated CO binds irreversibly to Cu_B; thus, the IR spectra of structures near Cu_B are perturbed as well. Inasmuch as H−Y is a ligand for Cu_B via the N_ϵ of H284, the IR spectrum of H−Y is very likely to be altered in the low-temperature photoproduct. The only tyrosine residue near the binuclear site is Y288; thus, any shifted tyrosine peaks are likely to be due to the "Y component" of H−Y. However, four histidines act as binuclear site ligands (H284, H333, and H334 for Cu_B plus H419 as the proximal histidine for the o_3 heme), and the two axial histidines (H106 and H421) of the *b* heme are not far away. Therefore, there must be additional evidence to definitively associate any observed histidine shifts with H−Y. To assist in the assignment of observed isotope shifts, we have performed normal mode calculations on a number of model structures including compound **5** and the five-residue helix turn of cytochrome bo_3 incorporating the C−N bond between the histidine and tyrosine ring structures. These models are useful primarily to identify the magnitude of the isotope shifts and localization of the vibrational modes; identification of absolute frequencies between ligation states may not be accurate in these models as the heme groups were not included. Also, as only one His fragment is included in these models, contributions from other ^{15}N-labeled His residues are not accounted for.

Spectra obtained from the low-temperature photolysis of CO-ligated cytochrome bo_3 with either natural abundance or ^{15}N-labeled histidine are shown in Figure 2. In these difference spectra, positive bands are associated with the Cu_B−CO state, while negative bands are due to the pre-photolysis Fe_{o_3}−CO state. For the purposes of identifying H−Y vibrational modes and to simplify the discussion, we will only refer to positive band positions, although the corresponding negative feature could be used for identification just as easily. There are at least four bands that appear shifted in the ^{15}N low-frequency spectrum (Figure 2a), one of which, at 1549 cm^{-1} in the NA spectrum, is very close in frequency to the peak in the H−Y model compound **5** that, as stated above, appears only in the covalently linked 4-methylimidazole, *p*-cresol structure. These observations indicate that the 1549 cm^{-1} feature may belong to H−Y in the enzyme. Note also that the 1549 cm^{-1} NA peak that is isotope shifted is concealed in the NA photochemical difference spectrum by a much more intense peak at 1552 cm^{-1}. The existence of the 1549 cm^{-1} peak is only discerned in the double (isotopic) difference spectrum between the photochemical difference spectra of the NA and ^{15}N enzymes (Figure 2). The assignment of the larger peak at 1552 cm^{-1}, which shows no isotope shift, is not clear, but possibilities include components of the amide II absorption due to peptide linkages near the binuclear site, or carboxylate asymmetric stretching modes (not, however, those of the heme propionates (*18*)).

Figure 3a shows data equivalent to those in Figure 2a except for d_4 substitution on tyrosine. One of the shifts discernible in the spectra is notable for being essentially identical to one observed in the ^{15}N case. That shift is in the NA mode at 1549 cm^{-1}, which, as in the ^{15}N spectrum, shifts to 1540 cm^{-1} in the d_4-Y isotopomer. There are two possible explanations for the correspondence between entirely different isotopomers: that it is a remarkable coincidence or that the 1549 cm^{-1} NA mode has a substantial contribution from the stretching motion of the inter-ring C−N bond, and that therefore the frequency is affected similarly by mass effects on either the H284 or Y288 ring. Convincing evidence supporting the latter scenario is provided by both experimental and computational results as is described below.

Table 1 lists the observed (bo_3) and calculated (five-residue helix) vibrational frequencies for modes in the 1400−1650 cm^{-1} range that display significant ^{15}N or ^{2}H shifts. There is a strong correlation between the observed and calculated values in all cases. The mode at 1549 cm^{-1} (calcd 1562 cm^{-1}), in particular, is the *only* mode that has a frequency near 1550 cm^{-1} and has *both* ^{15}N and ^{2}H shifts of appropriate magnitude. This mode is calculated to have substantial contribution from the C−N bond that forms the H−Y link

(see Figure 4). The observed ^{15}N and ^{2}H shifts for the 1549 cm^{-1} band could arise from this single vibrational mode.

Further evidence is provided by isotope shifts that are observed in the high-frequency region of the photochemical difference spectra, above 2800 cm^{-1}, where C−H and N−H stretching vibrations are expected. The relevant spectra are shown in Figures 2b and 3b for the NA, ^{15}N, and d_4-Y isotopomers. Prominent positive features appear in the spectrum of the NA enzyme at 3033 and 3135 cm^{-1}. The 3135 cm^{-1} NA peak appears at 3132 cm^{-1} in the ^{15}N enzyme and is essentially unshifted in the d_4-Y enzyme. The ^{15}N shift of 3 cm^{-1} is in the range expected for a C−H stretching mode in an imidazole ring upon changing the mass of the nitrogen atoms by 1 amu (note that the calculated diatomic shift in a 3100 cm^{-1} N−H stretching vibration as a result of exchanging ^{14}N for ^{15}N is much larger, ∼7 cm^{-1}). A peak near this frequency (ca. 3150 cm^{-1}) is present in the spectrum of the model compound **5** in D_2O, and calculated spectra show the primarily C−H stretches of imidazole rings shift by as much as 2 cm^{-1} upon ^{15}N substitution. Inasmuch as the cytochrome *bo*$_3$ spectra are also obtained in D_2O, and the 3135 cm^{-1} difference feature appears in every spectrum that we have recorded of heme−copper oxidases regardless of thorough H,D exchange and turnover (unpublished), we assign this peak to a stretching motion involving a nonexchangeable proton on a histidine imidazole ring, presumably a C_δ−H or C_ϵ−H stretch. However, we are unable to determine which of the histidine residues at the active site this mode is arising from.

The peak at 3033 cm^{-1} in the spectrum of the NA enzyme shifts to 3010 cm^{-1} in the ^{15}N spectrum. This 23 cm^{-1} shift is puzzling at first glance because it is far too large to be a simple ^{15}N mass effect on a N−H stretching mode (maximum diatomic shift ca. 7 cm^{-1}). This causes one to search for other sources of the shift, such as overtones, combination tones, or Fermi resonances involving the fundamental vibrations near 1500 cm^{-1}. Examining the NA fundamental vibrations in the ring mode region, only two of the frequencies add to give a predicted combination tone near 3033 cm^{-1}, the fundamental at 1549 cm^{-1}, and the fundamental at 1483 cm^{-1}, to give a predicted combination at 3032 cm^{-1}. The corresponding ^{15}N fundamental frequencies are at 1540 and 1473 cm^{-1} to give a predicted combination frequency of 3013 cm^{-1}, in excellent agreement with the observed high-frequency ^{15}N peak at 3010 cm^{-1}. We can confidently assign the 3033/3010 cm^{-1} ^{15}N-shifted pair to a combination tone involving the fundamentals noted above. Note that the IR results on the model compound **5** and normal mode calculations suggest that the 1549 cm^{-1} mode involves the inter-ring C−N stretching motion.

The peak at 3033 cm^{-1} is weaker than most of the fundamentals in the 1400−1600 cm^{-1} region by factors between 2 and 10. This makes it a very intense combination tone. In infrared spectroscopy, overtones and combination tones can only have intensity to the extent that the contributing fundamentals are anharmonic or anharmonically coupled. The high combination intensity in this case implies large anharmonic coupling of the fundamentals (which are not expected in themselves to be especially anharmonic). This coupling is most likely due to the torsional mode about the ring−ring H(N_ϵ)−Y(C_δ) bond. This torsion will be a low-energy high-amplitude motion which, because it changes the ring−ring H−Y dihedral angle, changes π overlap along the ring−ring bond and thus the force constant of this bond and also bonds within the H and Y rings, providing the requisite large anharmonic coupling.

The same *combination* tone must appear in the spectra of the d_4-Y isotopomer, and this is the case (Figure 3b). If the contributing *fundamentals* were localized on the imidazole ring, they would be insensitive to mass changes on the tyrosine ring and the d_4-Y combination would appear at the same frequency as in the NA spectrum. This would be the case if the shift in the 1549 cm^{-1} fundamental in the NA spectrum to 1540 cm^{-1} in the d_4-Y spectrum were simply coincidentally the same as the ^{15}N shift (i.e., if it were a totally different normal mode that did not combine with the imidazole ring modes). If, however, the d_4-Y shift occurs in the same mode as the ^{15}N shift, then the combination will also show the shifts due to deuteration of the tyrosine ring. This is expected if the 1549 cm^{-1} NA mode and the corresponding shifted modes indeed have substantial contribution from the inter-ring C−N bond in all three isotopomers. In this case it is reasonable for similar mass changes on either ring (in this case, 2 amu on H and 3 amu on Y) to result in similar shifts in the frequency of the inter-ring vibrational mode, as is predicted from our normal mode calculations.

The latter situation is actually observed, and this fact forms the basis for definitive assignment of the combination-forming fundamentals to the H−Y structure. As stated above, the 1549 cm^{-1} NA vibration shifts to 1540 cm^{-1} in the d_4-Y isotopomer. The 1483 cm^{-1} vibration is unshifted in the d_4-Y spectrum. If the 1540 cm^{-1} vibrations in the ^{15}N and d_4-Y isotopomer spectra are identical normal modes, the prediction is that the 3033 cm^{-1} combination tone in the NA spectrum should shift to 3024 cm^{-1} in the d_4-Y spectrum. The actual combination peak, in excellent agreement with this prediction, is observed at 3025 cm^{-1}.

The isotope shifts that we observe are in combination tones involving the same fundamental vibrations, but the mass substitutions are made on different substructures (in this case, H and Y). This can only occur if two requirements are met: (a) the substructures must be part of the same covalently bonded unit (viz., H−Y) and (b) at least one of the contributing fundamental modes must be shifted in frequency by mass effects on either substructure (i.e., the mode must have a substantial contribution from the inter-ring C−N bond). This allows us to assign definitively the NA vibrational frequencies at 1483 and 1549 cm^{-1} to modes of the H−Y structure, and the 1549 cm^{-1} vibration more specifically to a mode with a substantial contribution from the inter-ring bond. The calculated displacement vectors for these two modes are shown in Figure 4. The lower frequency mode is primarily localized on the His fragment, while the other (1549 cm^{-1}) contains contributions from both the His and Tyr rings and has a substantial C−N component.

Simultaneously with the initial submission of this paper, the Web version (subsequently in print (*28*)) of a paper by Hellwig et al. appeared. Comparison of these authors' results with ours is in order. There are no conflicts between the two papers, but there are many significant differences in how the measurements were made and what was observed. Hellwig et al. used the *Paracoccus denitrificans* cytochrome

oxidase, while ours is the *E. coli* quinol oxidase. Both depend on difference infrared spectral measurements on the enzyme, where the spectral differences are caused by a chemical perturbation. In our case the chemical perturbation was photodissociation of CO from the a_3 heme at 80 K, at which temperature the photodissociated CO binds irreversibly to Cu_B. In Hellwig et al. the perturbation is electrochemical oxidation of the metal centers of the enzyme at ambient temperature. Accordingly, there is no reason to expect the peak shifts observed by Hellwig at al. to be exactly the same as ours nor, in fact, that the same tyrosines will necessarily be involved. In our work, the photodissociation of CO is expected to exert its main effect on Y286 (Y280 in the *Pd* numbering), which is the only tyrosine near the proximal side of heme a_3, while the redox perturbation might affect at least four additional tyrosines, three located between the two hemes on the distal side of a_3 and one near Cu_A. The Hellwig measurements were made at pH 7 and 5 in H_2O; ours were at pH* 7.4 in D_2O.

Despite these differences, our results are remarkably similar. As expected from the temperature and the number of tyrosines observed, our double-difference spectrum (in our Figure 3) shows better spectral resolution than those of Hellwig et al. (in their Figure 3A), but the peaks observed in our spectra and theirs correspond almost feature for feature. The 1549 cm^{-1} difference feature that we consider to be highly significant is clearly evident (but, probably because these authors did not have the ^{15}N isotope information, not identified in the figure or in Table 1) in Figure 3A of Hellwig et al. (*28*). Also, we observed a peak (at 1522 cm^{-1} in WT and 1436 cm^{-1} in d_4-Y) that corresponds to Hellwig's 1524/1434 cm^{-1} pair, but we were unable to assign this peak (or its shift) because we did not have the mutant data in the work of Hellwig et al. (and because this peak does not isotope shift in the [$^{15}N_2$]His spectra (*24*)). Thus, in many respects, the results in these two papers are nicely complementary.

CONCLUSION

The findings described here provide specific guidance for the future use of infrared difference spectroscopy in providing direct, in situ spectroscopic evidence for radical formation involving the H−Y structure during the functional reactivity of the heme−copper oxidases. Specifically, the fundamental at 1549 cm^{-1} and the combination at 3033 cm^{-1} are identified as arising from vibrations which are localized on the H284−Y288 covalently bonded biring structure, and which contain a substantial contribution from the C−N bond between the two rings. It is expected that these vibrations will show a substantial frequency shift upon radical formation which should be observable, if it occurs, during the O_2 reduction cycle of the oxidases. While the other ^{15}N-shifted vibrations may belong to either H−Y or the other histidines near the binuclear site, the d_4-Y-shifted vibrations other than 1549 cm^{-1} are virtually certain to belong to Y288, the only tyrosine residue near the binuclear site.

ACKNOWLEDGMENT

Work at the Los Alamos National Laboratory was performed under the auspices of the U.S. Department of Energy. This work was done in collaboration with the National Stable Isotope Resource (P41 RR02231), an NIH/NCRR-supported research resource.

REFERENCES

1. Iwata, S., Ostermeier, C., Ludwig, B., and Michel, H. (1995) *Nature 376*, 660−669.
2. Soulimane, T., Gohlke, U., Huber, R., and Buse, G. (1995) *FEBS Lett. 368*, 132−134.
3. Tsukihara, T., Aoyama, H., Yamashita, E., Tomizaki, T., Yamaguchi, H., Shinzawa-Itoh, K., Nakashima, R., Yaono, R., and Yoshikawa, S. (1996) *Science 272*, 1136−1144.
4. Michel, H., Ostermeier, C., Iwata, S., and Harrenga, A. (1997) *FASEB J. 11*, 5−5.
5. Yoshikawa, S., Shinzawa-Itoh, K., Nakashima, R., Yaono, R., Yamashita, E., Inoue, N., Yao, M., Fei, M. J., Libeu, C. P., Mizushima, T., Yamaguchi, H., Tomizaki, T., and Tsukihara, T. (1998) *Science 280*, 1723−1729.
6. Iwata, S. (1998) *J. Biochem. 123*, 369−375.
7. Soulimane, T., Buse, G., Bourenkov, G. P., Bartunik, H. D., Huber, R., and Than, M. E. (2000) *EMBO J. 19*, 1766−1776.
8. Buse, G., Soulimane, T., Dewor, M., Meyer, H. E., and Bluggel, M. (1999) *Protein Sci. 8*, 985−990.
9. Davies, K. J. A., Delsignore, M. E., and Lin, S. W. (1987) *J. Biol. Chem. 262*, 9902−9907.
10. Blomberg, M. R. A., Siegbahn, P. E. M., Babcock, G. T., and Wikström, M. (2000) *J. Inorg. Biochem. 80*, 261−269.
11. Blomberg, M. R. A., Siegbahn, P. E. M., Babcock, G. T., and Wikström, M. (2000) *J. Am. Chem. Soc. 122*, 12848−12858.
12. Proshlyakov, D. A., Pressler, M. A., and Babcock, G. T. (1998) *Proc. Natl. Acad. Sci. U.S.A. 95*, 8020−8025.
13. Proshlyakov, D. A., Pressler, M. A., DeMaso, C., Leykam, J. F., DeWitt, D. L., and Babcock, G. T. (2000) *Science 290*, 1588−1591.
14. Puustinen, A., Bailey, J. A., Dyer, R. B., Mecklenburg, S. L., Wikström, M., and Woodruff, W. H. (1997) *Biochemistry 36*, 13195−13200.
15. Bailey, J. A., Tomson, F. L., Mecklenburg, S. L., MacDonald, G. M., Katsonouri, A., Puustinen, A., Gennis, R. B., Woodruff, W. H., and Dyer, R. B. (2002) *Biochemistry 41*, 2675−2683.
16. Lübben, M., and Gerwert, K. (1996) *FEBS Lett. 397*, 303−307.
17. Rost, B., Behr, J., Hellwig, P., Richter, O. M. H., Ludwig, B., Michel, H., and Mantele, W. (1999) *Biochemistry 38*, 7565−7571.
18. Behr, J., Hellwig, P., Mantele, W., and Michel, H. (1998) *Biochemistry 37*, 7400−7406.
19. Matney, T. S. (1964) *Biochem. Biophys. Res. Commun. 17*, 278−281.
20. Rumbley, J. N., Nickels, E. F., and Gennis, R. B. (1997) *Biochim. Biophys. Acta, Protein Struct. Mol. Enzymol. 1340*, 131−142.
21. Stewart, J. J. P. (1989) *J. Comput. Chem. 10*, 209−220.
22. Stewart, J. J. P. (1989) *J. Comput. Chem. 10*, 221−264.
23. Scott, A. P., and Radom, L. (1996) *J. Phys. Chem. 100*, 16502−16513.
24. McCauley, K. M., Vrtis, J. M., Dupont, J., and vanderDonk, W. A. (2000) *J. Am. Chem. Soc. 122*, 2403−2404.
25. Elliott, G. I., and Konopelski, J. P. (2000) *Org. Lett. 2*, 3055−3057.
26. Cappuccio, J. A., Ayala, I., Elliott, G. I., Szundi, I., Lewis, J., Konopelski, J. P., Barry, B. A., and Einarsdottir, O. (2002) *J. Am. Chem. Soc. 124*, 1750−1760.
27. Heitbrink, D., Sigurdson, H., Bolwien, C., Brzezinski, P., and Heberle, J. (2002) *Biophys. J. 82*, 1−10.
28. Hellwig, P., Pfitzner, U., Behr, J., Rost, B., Pesavento, R. P., von Donk, W., Gennis, R. B., Michel, H., Ludwig, B., and Mantele, W. (2002) *Biochemistry 41*, 9116−9125.

BI026370C